On the application of novel high temperature oxidation processes to enhance the performance of high voltage silicon carbide PiN diodes

Craig A. Fisher[1], Michael R. Jennings, Yogesh K. Sharma, Dean P. Hamilton,
Fan Li, Peter M. Gammon, Amador Pérez-Tomás, Stephen M. Thomas,
Susan E. Burrows and Philip A. Mawby
[1]School of Engineering
University of Warwick
Coventry, UK
Phone: +44 (0) 24-7655-1293
Fax: +44 (0) 24-7615-8922
Email: Craig.A.Fisher@warwick.ac.uk
URL: http://www.warwick.ac.uk

Acknowledgments

Keywords

<<Diode>>, <<Silicon carbide (SiC)>>, <<Semiconductor device>>, <<Wide band gap devices>>, <<Reverse recovery>>

Abstract

In this paper, the application of a combined high temperature ($1550°C$) thermal oxidation / annealing process has been applied to 4H-SiC PiN diodes with 110 μm thick n-type drift regions, for the purpose of increasing the carrier lifetime in the semiconductor. PiN diodes were fabricated on lifetime-enhanced 4H-SiC material, then were electrically characterised and compared against fabricated control sample PiN diodes. Forward current-voltage (I-V) measurements showed that the lifetime-enhanced devices typically had around 15% lower forward voltage drop and 40% lower differential on-resistance (at 100 A/cm^2 and 25°C) when compared against control sample PiN diodes. Reverse I-V measurements indicated that the reverse leakage current was strongly dependent on the active area, and hence perimeter-to-area ratio, of the fabricated devices, though large-area PiN diodes were measured to have a reverse leakage current density of around 1 nA/cm^2 (at 100 V reverse bias). Analysis of reverse recovery characteristics illustrated the excellent transient characteristics of both types of fabricated device, though, as expected from the increased carrier lifetime, the lifetime-enhanced PiN diodes had around 22% higher reverse recovery charge. The minority carrier lifetime was also extracted from reverse recovery characteristics; PiN diodes fabricated on the lifetime-enhanced 4H-SiC material were found to have a carrier lifetime over 35% higher than the control sample devices. Analysis of the overall power losses of both types of device found that the lifetime-enhanced PiN diodes typically dissipated around 40% less energy over the complete switching cycle than the control sample PiN diodes at 25°C.

Introduction

Due to its excellent electrical and thermal properties, 4H-silicon carbide (SiC) is widely expected to displace silicon (Si) for high voltage power electronics systems as we move into a lower carbon society. The material advantages of 4H-SiC include a critical electric field strength of ~2.5 MV/cm (approximately 10 times higher than Si), a thermal conductivity of ~3.7 W/cm-K (approximately 3 times that of Si), a band gap energy of 3.26 eV (approximately 3 times that of Si) and a saturation electron velocity of 2×10^7 cm/s (approximately twice that of Si) [1]. These superior material properties make 4H-SiC an ideal semiconductor material to provide the improvements in efficiency that are required for future power electronics systems as well as offering both higher voltage and higher temperature operating capability. Of particular relevance to high voltage systems are bipolar devices such as PiN diodes and Insulated Gate Bipolar Transistors (IGBTs). When compared to their unipolar counterparts, Schottky diodes and Metal Oxide Semiconductor Field-Effect Transistors (MOSFETs), these bipolar devices offer unparalled on-state efficiency for high voltage applications due to the conductivity modulation effect, which serves to lower the resistance of the thick, lowly-doped drift region required for blocking high voltages by injection of carriers from adjacent device regions.

The degree to which conductivity modulation enhances the on-state efficiency of bipolar power devices is heavily dependent on the carrier lifetime of the semiconductor material. Though in Si the carrier lifetime is sufficiently long to ensure effective conductivity modulation in the thick drift regions of high voltage devices (of the order of hundreds of microseconds), the carrier lifetime of as-grown 4H-SiC is significantly lower, with values up to 1 μs being typical [2]. For 4H-SiC devices intended to block 10 kV, a drift layer of around 100 μm is required, which in turn requires a carrier lifetime of around 5 μs for optimum performance. As such, it is clear that some form of post-growth carrier lifetime enhancement treatment is required for these high voltage devices.

It has been widely reported that the carrier lifetime in as-grown 4H-SiC is predominantly limited by the presence of the carbon vacancy-related $Z_{1/2}$ defect center in the material [3]. However, the carrier lifetime has been found to be dramatically enhanced by the use of thermal oxidation, which serves to 'repair' the $Z_{1/2}$ defect centers in the semiconductor bulk with carbon interstitials generated at the oxidised surface [4]. Unfortunately, with a conventional dry oxidation process, very long oxidation times are necessary to eliminate the $Z_{1/2}$ defect center in the thick epitaxial layers used for high voltage 4H-SiC devices, which results in a significant increase of the device processing cost. For instance, when performing the oxidation at 1300°C, the process takes over 50 hours when applied to a 100 μm thick epitaxial layer [5]. Moreover, the oxidation process is typically followed by a separate argon (Ar) annealing process to eliminate the HK0 defect center that is generated during the thermal oxidation [6], adding further processing complexity and cost. By using high temperature ($\geq$1400°C) oxidation processes, the oxidation rate is much higher and hence the oxidation time can be greatly reduced [7]. As such, the application of thermal oxidation at higher temperatures to realise long carrier lifetimes in high voltage 4H-SiC devices is attractive, and is investigated in this work.

Experimental details

Device fabrication

Figure 1 shows the cross-sectional schematic of the fabricated PiN diodes. The substrates employed for PiN diode fabrication in this work were n-type Si-face 4° off-axis 4H-SiC with a micropipe density of <1 per cm^2. An n-type buffer layer (0.5 μm at 1×10^{18} cm^{-3} doping concentration) was grown epitaxially on top of the substrate, followed by the n-type drift region (110 μm at 6×10^{14} cm^{-3}) and p-type anode (1 μm at $>1\times10^{19}$ cm^{-3}). After solvent- and acid-based cleaning, half of the samples underwent the lifetime-enhancing thermal oxidation / annealing process, which consisted of a thermal oxidation in pure dry O$_2$ at 1550°C for 15 minutes immediately followed by an Ar anneal at the same temperature for 30 minutes. This novel process is described in more detail in [8]. After carrying out this process, the thermally grown SiO$_2$ layer was removed. Individual device anodes were mesa isolated, with active areas ranging from 0.0011 to 0.0314 cm^2. Deposited tetraethyl orthosilicate (TEOS) SiO$_2$ was used for surface passivation, and an optimised titanium (Ti) / aluminum (Al) ohmic contact was used for the anode [9]. A Ti / nickel (Ni) ohmic contact was used for the cathode, and thick layers of Al and silver (Ag) were deposited onto the front and back sides of the dies respectively, to enable wire bonding and soldering to direct copper bond (DCB) substrates.
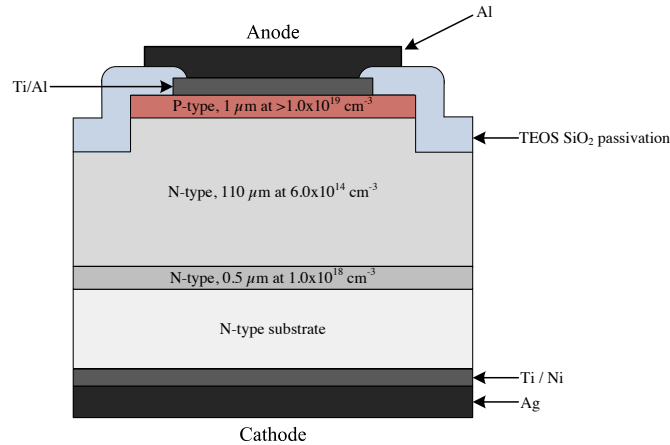
Figure 1: Cross-sectional schematic of fabricated PiN diodes.

Device packaging

After completion of device fabrication and on-die probe testing, each die has been soldered onto an aluminium nitride (AlN) direct copper bond (DCB) substrate using a high temperature solder. Spade terminals for connecting each device anode have also been soldered onto the DCB. Wire bonding from the Al anode contact pads to the spade terminals has been performed using an ultrasonic wire bonder with 25 μm Al wire. In order to minimise the effects of wire bond resistance and inductance, up to 10 bonds were wired in parallel for each diode, depending on the device active area. A photograph of a DCB-mounted PiN diode die is shown in Figure 2. Each die contains four PiN diodes of varying active areas, in addition to conventional transfer length method (TLM) and circular TLM structures for extracting the p-type anode ohmic contact resistance [10].
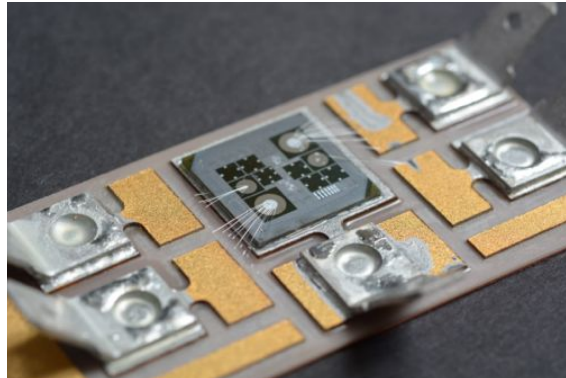
Figure 2: Photograph of fabricated PiN diode die.

Test setup

Forward I-V characterisation

For on-die testing of forward current-voltage (I-V) characteristics of the fabricated PiN diodes, a Keithley 4200-SCS semiconductor parameter analyser system has been used in conjunction with a heated chuck and probe station. The use of a heated chuck has enabled device characteristics at temperatures ranging from 25°C to 300°C to be obtained. Packaged devices have been tested using a Tektronix 371B high power curve tracer. In order to minimise device self-heating effects during testing, pulsed measurement mode has been used in both measurement setups.

Reverse I-V characterisation

On-die reverse leakage current measurements (up to 100 V reverse bias) of the fabricated PiN diodes have been obtained under low-noise, dark conditions using an Agilent B1500A semiconductor parameter analyser in conjunction with a probe station. Reverse breakdown measurements were performed on DCB-mounted devices using a Tektronix 371B high power curve tracer.

Switching (reverse recovery) characterisation

In order to characterise the reverse recovery performance of the fabricated PiN diodes, a custom-built clamped inductive switching test rig has been employed. Characteristics at temperatures up to 125°C have been obtained by heating an inert fluid in which the devices under test are submerged. The test rig is based on a chopper cell circuit, shown schematically in Figure 3. This circuit is operated in double-pulse mode which operates as follows: the gate of the IGBT is first pulsed on for a duration ΔT, allowing the inductor current to build up to the desired level. Once this current level is reached, the IGBT is turned off, forcing the inductor current to flow through the diode, turning it on, and allowing the IGBT to support a voltage across the collector-emitter junction (V_{CE}). After a short duration t_{off}, the gate of the IGBT is pulsed on for a second time; due to the removal of stored charge in the PiN diode a reverse recovery current flows through the diode until it can support the reverse voltage.
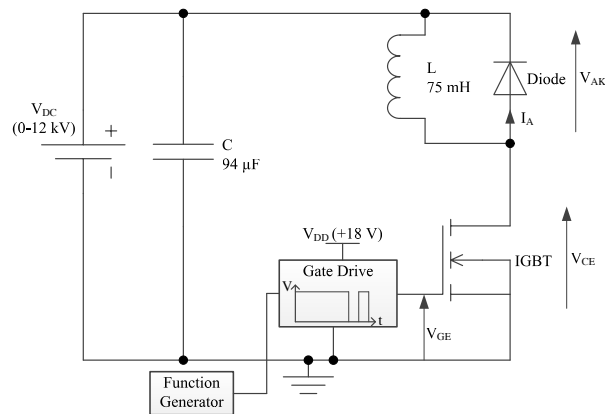

Figure 3: Schematic of chopper cell circuit used for clamped inductive switching tests.

Results and discussion

Forward I-V characteristics

The typical forward I(J)-V characteristics of the fabricated PiN diodes measured across the temperature range 25°C and 300°C are shown in Figure 4. It is clearly evident from this Figure that both types of PiN diode exhibit a negative temperature coefficient; this is the result of several competing physical mechanisms. Though the carrier mobility decreases at elevated temperature due to increased lattice scattering, reducing the conductivity of the semiconductor, this is outweighed by increasing dopant ionisation in the p-type anode (and thus increased carrier injection into the drift region) and lower ohmic contact resistances [11]. In addition, the turn-on voltage of the *pn* junction is decreased, as the intrinsic carrier concentration n_i increases with temperature. However, it is noted that beyond 150°C, the di/dv is approximately the same beyond the point of turn-on, indicating that the effects of increased dopant ionisation and reduced ohmic contact resistances are balanced by the effect of reduced carrier mobility. The difference in characteristics between the lifetime-enhanced and the control sample PiN diodes is clearly significant, with forward voltage drops of 3.81 V and 4.45 V respectively (at 100 A/cm^2 and 25°C), an improvement of around 15% for the lifetime-enhanced devices. It is noted that this improvement is approximately constant across the measurement temperature range.
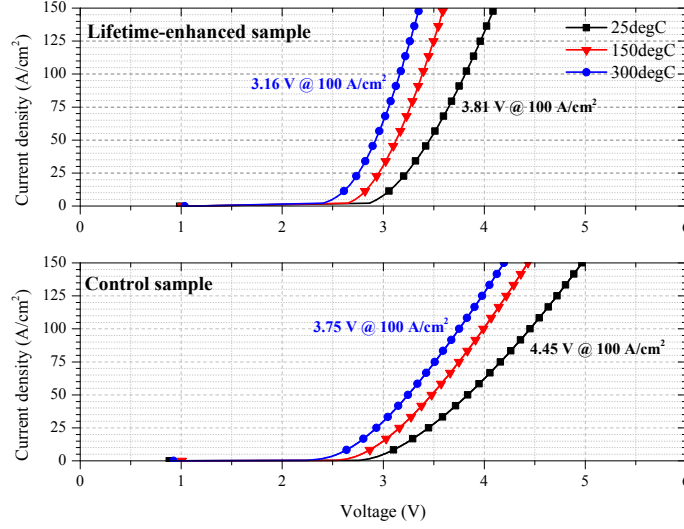
Figure 4: Typical forward J-V characteristics for control sample (bottom) and lifetime-enhanced (top) PiN diodes.

Fig. 5 shows the typical differential on-resistance ($R_{on,diff}$) as a function of current density of both the lifetime-enhanced PiN diodes and the control sample PiN diodes across the temperature range 25°C to 300°C, calculated from

$$R_{on,diff} = \frac{dV}{dJ_F} \qquad (1)$$

In both devices, the $R_{on,diff}$ is initially high at low biases, then rapidly decreases with increasing bias as carriers are injected from both emitters into the drift region. The lifetime-enhanced PiN diode again shows improved characteristics in comparison with the control sample PiN diode, with $R_{on,diff} =$ 6.2 mΩ-cm^2 at 100 A/cm^2 and 25°C compared to 11.0 mΩ-cm^2 for the control sample device. This equates to a decrease in $R_{on,diff}$ of around 40% for the lifetime-enhanced devices.

Reverse I-V characteristics

The reverse leakage current characteristics of the fabricated PiN diodes are shown in Figure 6. Although it is expected that with an increased carrier lifetime a lower reverse leakage current would be observed due to the reduced carrier generation rate [12], it is evident from this Figure that the reverse leakage current is dominated by the active area of the device, with the small-area devices (0.0011 cm^2) having a larger leakage current than the large-area devices (0.0314 cm^2). This is attributed to the high perimeter-to-area ratio of the small-area devices, as recombination-generation defect centres are expected near the etched mesa sidewall [13]. However, in terms of an actual high voltage power electronics application, large-area 4H-SiC devices will be used in order to provide the required current capacity; as such, these small-area effects can be neglected. Low reverse leakage current densities of around 1 nA/cm^2 (at 100 V reverse bias and 25°C) have been achieved for the large-area devices.
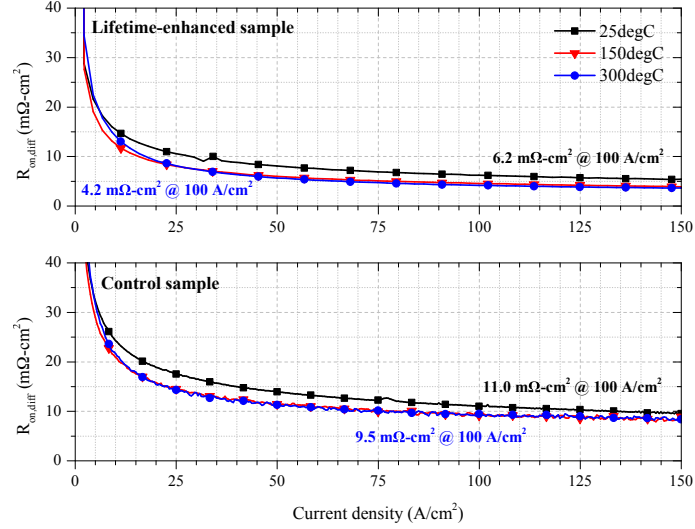
Figure 5: Typical differential on-resistance as a function of current density for control sample (bottom) and lifetime-enhanced (top) PiN diodes.

Switching (reverse recovery) characteristics

Figure 7 shows the reverse recovery characteristics of the fabricated PiN diodes between 25°C and 125°C. It is noted that, due to the fact that the devices were fabricated with no edge termination, a relatively low DC bus voltage of 100 V has been used for these tests. Though this means that the transient power losses presented here are not representative of the intended application for these PiN diodes, it still allows a valid quantitative comparison to be made between the lifetime-enhanced and the control sample devices. It is clear from this Figure that the transient characteristics of both types of device deteriorate with increasing temperature (both the peak reverse current density J_{RP} and the reverse recovery time t_{rr} increase); this is expected as the carrier lifetime, and thus the stored charge in the drift region, increases with temperature. It is also evident that the lifetime-enhanced devices exhibit marginally worse transient characteristics, indicating a longer carrier lifetime. As outlined in [14], the high-level carrier lifetime τ_{HL} can be estimated from

$$\tau_{HL} = 2 \cdot \frac{I_{RP}}{I_F} \cdot t_{rr} \qquad (2)$$

where I_F is the diode forward current. Using this equation, a value of τ_{HL} of 1.2 μs was extracted for the lifetime-enhanced PiN diodes; this compared to a value of 750 ns for the control sample PiN diodes, an increase of over 35%. This increased carrier lifetime meant that, the lifetime-enhanced PiN diodes had a reverse recovery charge Q_{rr} of 67 nC, compared to 52 nC for the control sample PiN diode, an increase of around 22%. For comparison, a commercial 6.5 kV Si PiN diode was found to have $Q_{rr} =$ 575 nC under identical test conditions; this illustrates the excellent transient performance of the 4H-SiC PiN diodes.
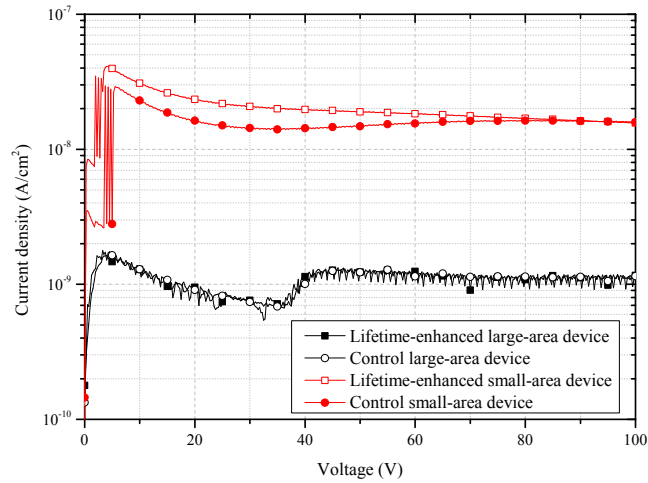
Figure 6: Reverse leakage currents of lifetime-enhanced and control sample PiN diodes. Both small- and large-area device characteristics are shown.
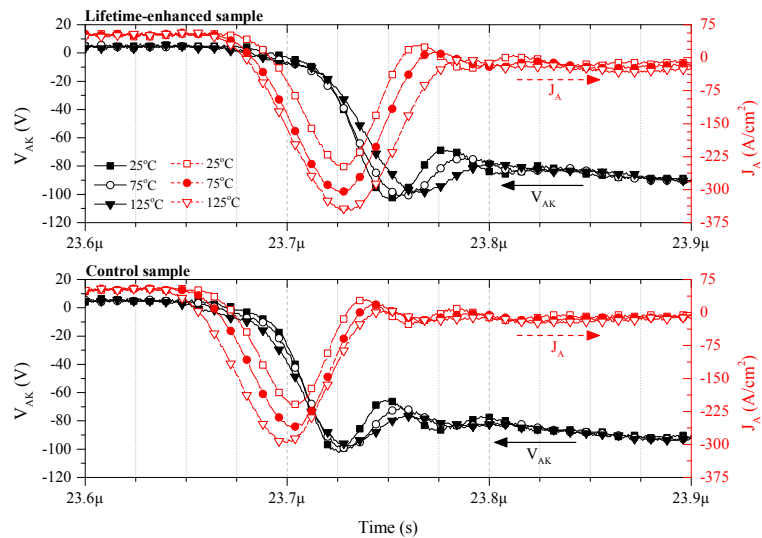

Figure 7: Reverse leakage currents of lifetime-enhanced and control sample PiN diodes. Both small- and large-area device characteristics are shown.

Analysis of device power losses

In order to evaluate the overall performance benefits that are provided by the lifetime-enhancing fabrication process, the total energy losses over the complete switching cycle have been analysed. Figures 8 and 9 show the energy losses across the temperature range 25°C to 125°C for a typical control sample and lifetime-enhanced PiN diode respectively. It is evident that in both types of device, the turn-on energies are negligible, irrespective of measurement temperature. In the control sample PiN diode, the overall

energy losses are clearly dominated by the conduction losses, which are around 940 nJ at 25°C and decrease to around 830 nJ at 125°C. The turn-off losses are relatively small, around 170 nJ at 25°C and increasing to around 300 nJ at 125°C. As such, the total energy losses of the control sample PiN diode remain approximately constant over the measured temperature range, at around 1.1 μJ. In contrast, the conduction losses of the lifetime-enhanced PiN diode are around 450 nJ at 25°C, decreasing to around 350 nJ at 125°C. The turn-off losses are slightly lower, at around 220 nJ at 25°C, and increase to around 470 nJ at 125°C. This results in a total energy loss over the complete switching cycle of around 690 nJ at 25°C and 830 nJ at 125°C. From this analysis, it can be seen that the lifetime-enhanced PiN diodes offer an overall power loss reduction of around 40% at 25°C, and 27% at 125°C.
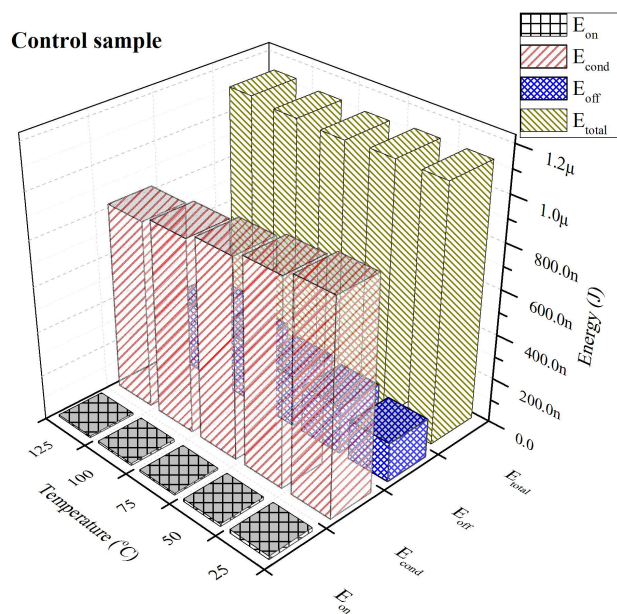

Figure 8: Total energy dissipated for the control sample PiN diode across the temperature range 25°C to 125°C.

Conclusions and future work

In this paper, the electrical performance of lifetime-enhanced 4H-SiC PiN diodes with 110 μm thick n-type drift regions has been presented and compared to control sample PiN diodes. Lifetime-enhancement was achieved using a high temperature thermal oxidation and annealing process, previously reported by the authors in [8]. Forward I-V characterisation showed that the lifetime-enhanced PiN diodes had a typical forward voltage drop of around 3.8 V and a differential on-resistance of 6.2 mΩ-cm^2 at 100 A/cm^2 and 25°C; this equated to improvements of around 15% and 40% respectively, compared to the control sample PiN diodes. Reverse I-V characterisation showed that the reverse leakage currents were slightly lower in the lifetime-enhanced PiN diodes for a given device active area, though the reverse leakage current was found to be proportional to the perimeter-to-area ratio of the devices, due to enhanced generation at the etched sidewall of the PiN diodes. Large-area devices were found to have reverse leakage current densities of the order 1 nA/cm^2 at 100 V reverse bias and 25°C. Reverse recovery characterisation illustrated the excellent transient performance of the fabricated 4H-SiC PiN diodes, with a typical lifetime-enhanced PiN diode having a reverse recovery charge of 67 nC. This was approximately 22% higher than that for the control sample PiN diode, due to the increased carrier lifetime. The carrier lifetime was extracted from the reverse recovery characteristics; PiN diodes fabricated on the lifetime-enhanced 4H-SiC material were found to have a carrier lifetime of 1.2 μs, which was over 35% higher than the control sample PiN diodes. Finally, analysis of power losses showed that, over the complete switching cycle, the lifetime-enhanced PiN diodes dissipated around 40% less energy than the control sample devices. As such, we have shown that the lifetime-enhancing fabrication process applied to the PiN diodes fabricated in this work is hugely beneficial for improving their electrical performance. Moreover, this process could also be applied to other bipolar 4H-SiC devices, in order to realise significant loss reduction in power electronics systems.
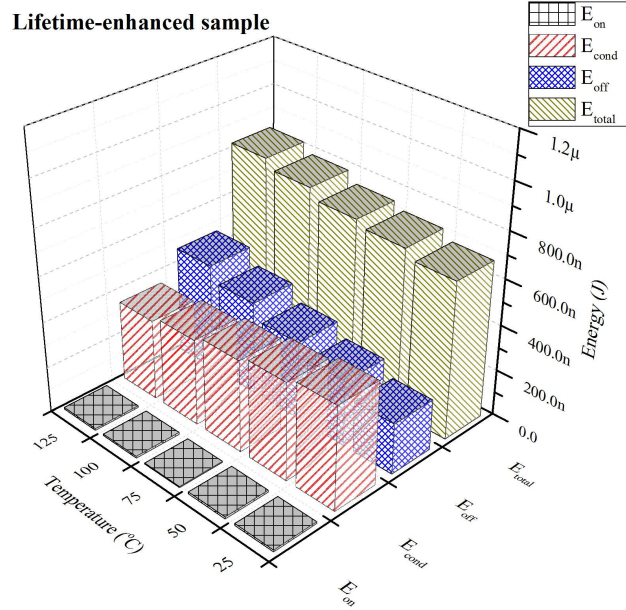
Figure 9: Total energy dissipated for the lifetime-enhanced PiN diode across the temperature range 25°C to 125°C.

References

[1] Chow T. P.: Mater. Sci. Forum Vol 778-780, pp. 1077-1082, 2014.

[2] Hiyoshi T. and Kimoto T.: Appl. Phys. Expr. Vol 2, 041101, 2009.

[3] Kimoto T. et al.: Phys. Stat. Sol. (b) Vol 425 no. 7, pp. 1327-1336, 2008.

[4] Ichikawa S. et al.: Appl. Phys. Expr. Vol 5, 101301, 2012.

[5] Kawahara K. et al.: Mater. Sci. Forum Vol 717-720, pp. 241-244, 2012.

[6] Hiyoshi T. and Kimoto T.: Appl. Phys. Expr. Vol 2, 091101, 2009.

[7] Thomas S. M. et al.: Mater. Sci. Forum Vol 778-780, pp. 599-602, 2014.

[8] Fisher C. A. et al.: Accepted for publication in IEEE Trans. Semicon. Man., (notified April 2014).

[9] Jennings M. R. et al.: Mater. Sci. Forum Vol 778-780, pp. 693-696, 2014.

[10] Schroder D. K.: Semiconductor Material and Device Characterization - Third Edition, John Wiley and Sons, Hoboken, NJ, USA, 2006.

[11] Fisher C. A. et al.: Mater. Sci. Forum Vol 717-720, pp. 993-996, 2012.

[12] Baliga B. J.: Fundamentals of Power Semiconductor Devices, Springer, NY, USA, 2008.

[13] Losee P.: Ph.D. dissertation, Rensselaer Polytechnic Institute, Troy, NY, USA, 2007.

[14] Nakayama K.: IEEE Trans. Electron Devices Vol 59 no. 4, pp. 895-901, 2012.